remote sensing

MDPI

Article

Influence of the Nocturnal Effect on the Estimated Global CO_2 Flux

Rui Jin [1], Tan Yu [1,*], Bangyi Tao [2], Weizeng Shao [1,3], Song Hu [1] and Yongliang Wei [1]

[1] College of Marine Sciences, Shanghai Ocean University, Shanghai 201306, China; m200200561@st.shou.edu.cn (R.J.); shaoweizeng@mail.tsinghua.edu.cn (W.S.); shu@shou.edu.cn (S.H.); yl-wei@shou.edu.cn (Y.W.)

[2] State Key Laboratory of Satellite Ocean Environment Dynamics, Second Institute of Oceanography, Ministry of Natural Resources, Hangzhou 310012, China; taobangyi@sio.org.cn

[3] National Satellite Ocean Application Service, Ministry of Natural Resources, Beijing 100081, China

* Correspondence: tyu@shou.edu.cn; Tel.: +86-021-6190-0169

Abstract: We found that significant errors occurred when diurnal data instead of diurnal–nocturnal data were used to calculate the daily sea-air CO_2 flux (F). As the errors were mainly associated with the partial pressure of CO_2 in seawater (pCO_{2w}) and the sea surface temperature (SST) in the control experiment, pCO_{2w} and SST equations were established, which are called the nocturnal effect of the CO_2 flux. The root-mean-square error between the real daily CO_2 flux (F_{real}) and the daily CO_2 flux corrected for the nocturnal effect (F_{com}) was 11.93 mmol m^{-2} d^{-1}, which was significantly lower than that between the F_{real} value and the diurnal CO_2 flux (F_{day}) (46.32 mmol m^{-2} d^{-1}). Thus, the errors associated with using diurnal data to calculate the CO_2 flux can be reduced by accounting for the nocturnal effect. The mean global daily CO_2 flux estimated based on the nocturnal effect and the sub-regional pCO_{2w} algorithm (cor_F_{com}) was −6.86 mol m^{-2} y^{-1} (September 2020–August 2021), which was greater by 0.75 mol m^{-2} y^{-1} than that based solely on the sub-regional pCO_{2w} algorithm (day_F_{com} = −7.61 mol m^{-2} y^{-1}). That is, compared with cor_F_{com}, the global day_F_{com} value overestimated the CO_2 sink of the global ocean by 10.89%.

Keywords: daytime data; CO_2 flux; partial pressure; nocturnal effect; ocean sink

check for updates

Citation: Jin, R.; Yu, T.; Tao, B.; Shao, W.; Hu, S.; Wei, Y. Influence of the Nocturnal Effect on the Estimated Global CO_2 Flux. *Remote Sens.* **2022**, *14*, 3192. https://doi.org/10.3390/rs14133192

Academic Editors: Yunjun Yao, Gad Levy, Xiaotong Zhang, Kun Jia and Ayad M. Fadhil Al-Quraishi

Received: 9 May 2022
Accepted: 1 July 2022
Published: 3 July 2022
Corrected: 19 December 2022

1. Introduction

Since the beginning of the Industrial Revolution, human activities such as fossil fuel combustion, cement production, and land-use change have released large amounts of carbon dioxide (CO_2) into the atmosphere, thus disrupting the global carbon cycle and causing global climate change [1]. As an important reservoir of carbon, the oceans currently absorb approximately 25% of anthropogenic CO_2 emissions [2]. Although this could reach 70–80% on a timescale of a few hundred years and 80–95% on a timescale of a few thousand years, these estimates remain uncertain [3]. Some studies have suggested that the estimated errors associated with the partial pressure of CO_2 (pCO_2) are mainly at the regional level, corresponding to a difference of >10% of the mean climatic pCO_2, which is an order of magnitude greater than the uncertainty associated with the most advanced measurements. Yu (2014) found that a different CO_2 transfer velocity led to considerable uncertainty in the estimated global CO_2 flux [4]. Therefore, it is critical to reduce the uncertainty associated with the estimated oceanic CO_2 flux to improve our understanding of the potential processes that control the distribution of anthropogenic CO_2 between the atmosphere, land, and oceans in the present and future [5].

At present, the sea–air CO_2 flux can be measured directly using the eddy correlation method. Alternatively, the CO_2 flux is often calculated by the block method formula [4], as follows: sea–air CO_2 flux = sea–air gas transfer velocity × solubility of CO_2 in seawater × (pCO_2 in seawater–pCO_2 in air). If the CO_2 flux is positive, it means that CO_2

enters the atmosphere from the ocean, i.e., the ocean is the source of CO_2. If theCO_2 flux is negative, it means that CO_2 enters the ocean from the atmosphere, i.e., the ocean is the sink of CO_2. These parameters are obtained by remote sensing.

The algorithm for determining the pCO_2 of seawater based on remote sensing data mainly depends on the sea temperature (*SST*) and chlorophyll-a (*Chl-a*) concentration. Bai et al. (2015) used the relationship between these factors and the pCO_2 of seawater to establish the corresponding algorithm [6]. As *SST* and *Chl-a* data are mainly obtained using optical remote-sensing techniques, there are no nocturnal data; however, some researchers consider that the diurnal–nocturnal variations in *SST* and *Chl-a* are significant.

Stuart-Menteth et al. (2003) and Genemann et al. (2003) analysed *SST* data measured at mooring buoys and observed a significant daily variation in *SST*, which may have been due to the diurnal–nocturnal variation in solar radiation, wind stress, and cloud cover [7–9]. Lu (2007) observed a positive correlation between the daily variations in the pCO_2 of seawater and the *SST* [10]. Jeffery et al. (2007) found that the daily variation in the *SST* significantly affected the sea–air exchange of CO_2, increasing the emission of air from the ocean and reducing the pCO_2 of seawater, especially at the equator. The *SST* affects the CO_2 flux by influencing the pCO_2 of seawater and the solubility of CO_2 at low wind speeds [9,11]. When the reference temperature is 20 °C, the effect of the *SST* on solubility accounts for ~2.7% of the total variation in the CO_2 flux [12]. At high latitudes, as the solubility of CO_2 increases at low temperatures, the daily variation in salinity alters the ability of the oceans to absorb atmospheric CO_2 [13].

Marrec et al. (2014) and Borges et al. (1999) concluded that the tidal cycle affected the daily variation in phytoplankton abundance, and thus the daily variation in the pCO_2 of seawater [14,15]. Bates et al. (2001) argued that the extremely high productivity of organisms in coral reef ecosystems could also cause large daily variations in the pCO_2 of seawater [16]. Moreover, the daily variation in the pCO_2 of seawater is influenced by biological activity, whereby CO_2 is mainly consumed as a result of photosynthesis during the day and released due to respiration at night [17]. Marrec et al. (2014) estimated that the mean diurnal–nocturnal variation in the pCO_2 associated with the biological cycle accounted for 16% of the mean CO_2 sink [14].

In addition to *SST* and biological activity, Kuss et al. (2006) found that the water mass mixing process was one of the main factors controlling the variation in the pCO_2 of surface seawater, while the daily variation in the wind speed affected the water mass mixing process [18–21]. Jeffery et al. (2007) found that the diurnal–nocturnal variation in seawater convection also affected the sea–air CO_2 transfer velocity and the daily variation in the sea–air CO_2 flux [11,22,23]. Rousseau et al. (2020) observed that the daily variation in the atmospheric CO_2 concentration directly affected the pCO_2 of seawater [24]. Furthermore, the change in the pCO_2 of air affected the CO_2 flux. Figure 1 depicts the effects of these factors on the sea–air CO_2 flux.

As there is a clear diurnal–nocturnal variation in the pCO_2 of seawater, it is inaccurate to use solely diurnal data instead of diurnal–nocturnal data. One of the goals of this study was that the relationship between the diurnal pCO_2 and nocturnal pCO_2 was determined and used to revise the pCO_2 calculated based on diurnal data only. In addition to this, it is also our goal to determine the relationships between diurnal and nocturnal data for the other parameters involved in the CO_2 flux block method and to use the corresponding relationships to correct the diurnal data for each parameter. Ultimately improving the accuracy of the global CO_2 flux estimates by considering the diurnal variation of parameters.

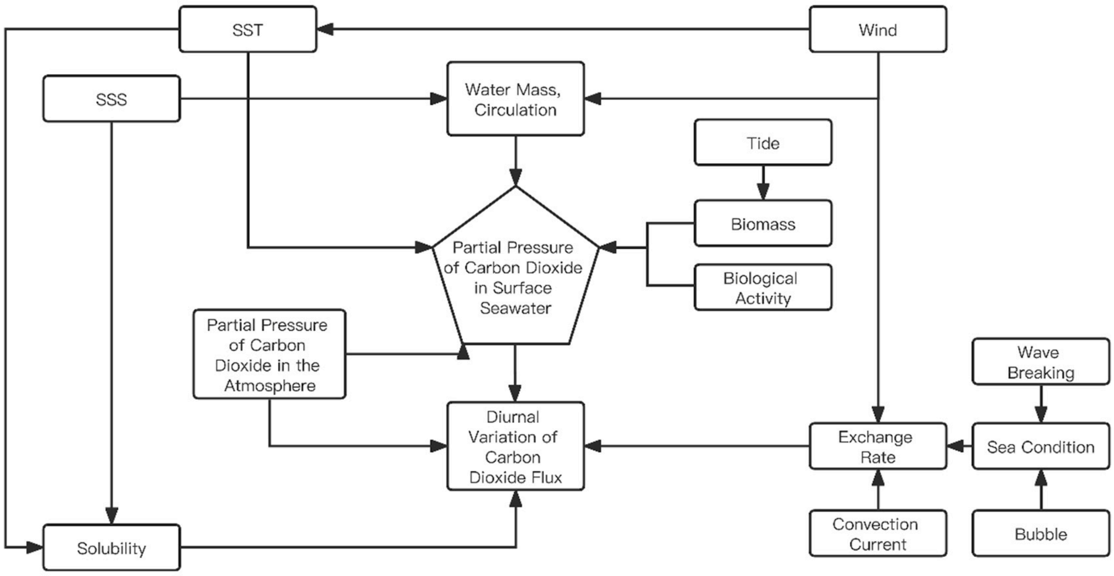

Figure 1. Schematic of the factors influencing the sea–air CO_2 flux.

2. Data and Methods

2.1. Buoy Data

The pCO_2, *SST*, and sea surface salinity (*SSS*) data used in this study were obtained from the global CO_2 time series and mooring project of the Ocean Carbon Data System (OCADS) (https://www.ncei.noaa.gov/access/ocean-carbon-data-system/oceans/time_series_moorings.html, accessed on 8 May 2022). International organisations from 18 countries have installed sensors on moored buoys to provide high-resolution time series measurements of the pCO_2 of the atmospheric boundary layer and ocean surface. Time series and mooring projects on CO_2 are coordinated by the International Ocean Carbon Coordination Project (IOCCP) and OceanSITES.

Figure 2 shows a map of the buoy stations, where data are taken at 00:00, 03:00, 06:00, 09:00, 12:00, 15:00, 18:00, and 21:00. In Figure 3, the period 2010 to 2020 has the largest number of buoy stations, so we chose this time range as the study time in our study.

2.2. Satellite Remote Sensing Data

2.2.1. Wind Data and Atmospheric Pressure Data

Wind and atmospheric pressure data from 2010 to 2020 were obtained from ERA5 (https://cds.climate.copernicus.eu/cdsapp#!/dataset/reanalysis-era5-single-levels?tab=overview, accessed on 8 May 2022), which is the fifth-generation European Centre for Medium-Range Weather Forecasts (ECMWF) reanalysis of global climate and weather over the past 4–7 years. We used the u and v components of the wind speed (m s^{-1}) at a height of 10 m above the Earth's surface, with a time resolution of 1 h and a spatial resolution of $0.25° \times 0.25°$. To correspond to the pCO_2, *SST*, and *SSS* data of the buoys, wind and atmospheric pressure data at 00:00, 03:00, 06:00, 09:00, 12:00, 15:00, 18:00, and 21:00 were selected.

2.2.2. *SST* and *Chl-a* Data

The *SST* and *Chl-a* data used in this study were obtained from the Aqua MODIS global map 11-µm daytime *SST* and *Chl-a* data (version R2019.0, https://oceandata.sci.gsfc.nasa.gov/directdataaccess/Level-3%20Mapped/Aqua-MODIS, accessed on 8 May 2022) for the period June 2020 to May 2021 at a temporal resolution of 1 day and a spatial resolution of 4 km $\times$ 4 km.

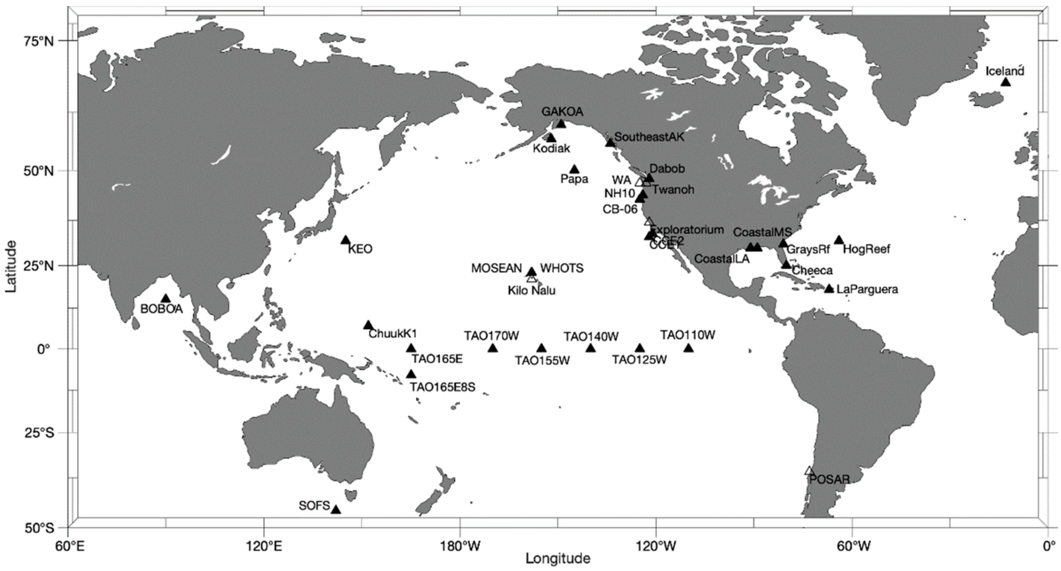

Figure 2. Map of global buoy stations. ▲ indicates the selected stations for this study.

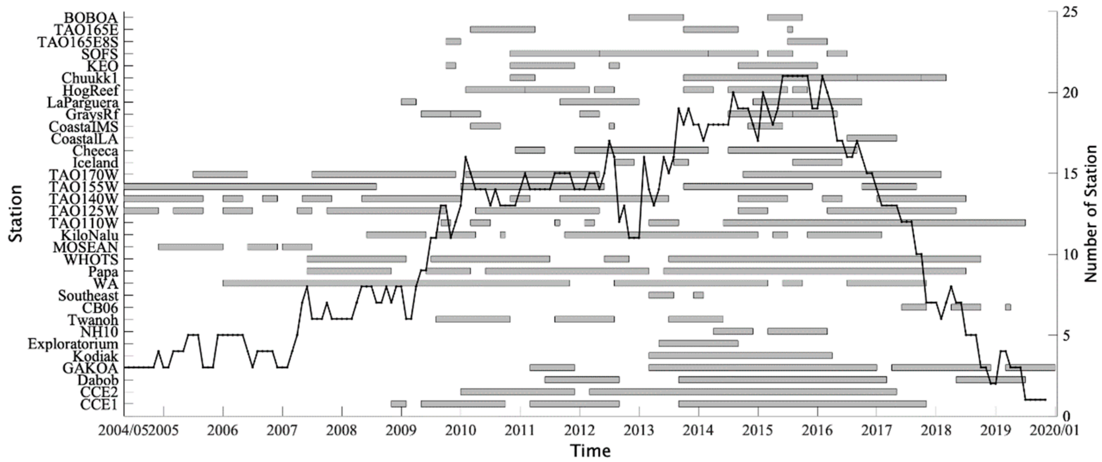

Figure 3. Time series of global buoy data. The right axis shows the number of stations corresponding to a given time. The horizontal bars represent the data available at the corresponding site at different times.

2.2.3. *SSS* Data

The *SSS* data were obtained from the 10-day 3D global ocean forecast data (spatial resolution of 0.083° × 0.083°), which are updated daily at 00:00, 06:00, 12:00, and 18:00 by the global ocean analysis and prediction system (https://resources.marine.copernicus.eu/product-detail/GLOBAL_ANALYSIS_FORECAST_PHY_001_024/INFORMATION, accessed on 8 May 2022).

2.2.4. Carbon Dioxide and Water Vapour Data

The atmospheric CO_2 concentration and water vapour data were obtained from Aqua AIRS IR-only Level 3 climcaps (gridded daily V2 with integrated quality control), with two daily tracks divided into diurnal and nocturnal data with a spatial resolution of 1° × 1° (https://disc.gsfc.nasa.gov/datasets/SNDRAQIL3CDCCP_2/summary?keywords=CO2, accessed on 8 May 2022).

2.3. Calculation of the CO_2 Flux

The block formula of the sea–air CO_2 flux [25], F (mmol m^{-2} d^{-1} or mol m^{-2} s^{-1}), is as follows:

$$F = kL\Delta pCO_2 \quad (1)$$

When the atmospheric CO_2 concentration is high, CO_2 moves from the atmosphere to the ocean; thus, F is negative. The direction of F is determined by the difference between the pCO_2 of seawater and air (i.e., ΔpCO_2) [26], which is usually expressed in units of µatm and is calculated using Equation (2):

$$\Delta pCO_2 = pCO_{2\mathrm{w}} - pCO_{2\mathrm{a}} \quad (2)$$

where $pCO_{2\mathrm{w}}$ is the pCO_2 of seawater (in Pa or µatm) and $pCO_{2\mathrm{a}}$ is the pCO_2 of air (in Pa or µatm).

The sea–air gas transfer velocity, k (cm h^{-1}), is expressed as follows [27]:

$$k = 0.251U_{10}^2(Sc/660)^{-0.5} \quad (3)$$

where U_{10} is the wind speed (m s^{-1}) at a height of 10 m above sea level and $Sc = A + Bt + Ct^2 + Dt^3 + Et^4$ (t is the temperature in °C; A = 1923.6, B = −125.06, C = 4.3773, D = −0.085681, and E = 0.00070284).

The solubility of CO_2 in seawater, L (mol L^{-1} atm^{-1}), was calculated using Weiss' formula [28]:

$$\begin{aligned} \ln L = A_1 + A_2(100/SST) + A_3 \ln(SST/100) + \\ SSS‰\left[B_1 + B_2(SST/100) + B_3(SST/100)^2\right] \end{aligned} \quad (4)$$

where SST is the absolute SST (in K) (absolute $SST = t$ (°C) + 273.15), SSS is the surface seawater salinity, A_1 = −58.0931, A_2 = 90.5069, A_3 = 22.294, B_1 = 0.027766, B_2 = −0.025888, and B_3 = 0.0050578.

3. Results and Discussion

3.1. Estimated Daily Variation in the CO_2 Flux

Figure 4 shows that there was a significant diurnal–nocturnal variation in the sea–air CO_2 flux. As the sea–air CO_2 flux is usually estimated using diurnal remote sensing data, we studied the difference between the CO_2 flux calculated using (i) diurnal data (F_{day}) only and (ii) diurnal–nocturnal data (F_{real}). There was a significant difference between the F_{day} and F_{real} values (Figure 5). The largest difference was observed at HogReef station (64°W, 32°N), where F_{real} was 4.31 mmol m^{-2} d^{-1} lower than F_{day} on average. In contrast, the smallest difference was observed at BOBOA station (90°E, 15°N), where F_{real} was 0.01 mmol m^{-2} d^{-1} lower than F_{day}. Of the stations where F_{real} was larger than F_{day}, CoastalMS (88°W, 30°N) had the largest $F_{real} - F_{day}$ value of 2.64 mmol m^{-2} d^{-1}. Temporally, the largest difference was observed in 2018 (data for 2020 were sparse and not included in the comparison), whereas the smallest difference was observed in 2011. The largest difference was observed on 27 August 2018, when F_{real} was 21.90 mmol m^{-2} d^{-1} lower than F_{day}. The smallest difference was observed on 27 July 2011, when F_{real} was 1.69×10^{-5} mmol m^{-2} d^{-1} higher than F_{day}. The average difference across the period from 2010 to 2020 was 0.16 mmol m^{-2} d^{-1}. Therefore, using diurnal data instead of diurnal–nocturnal data to calculate the CO_2 flux will cause significant errors in the calculation of the daily CO_2 flux. Accordingly, this study attempts to eliminate such errors.

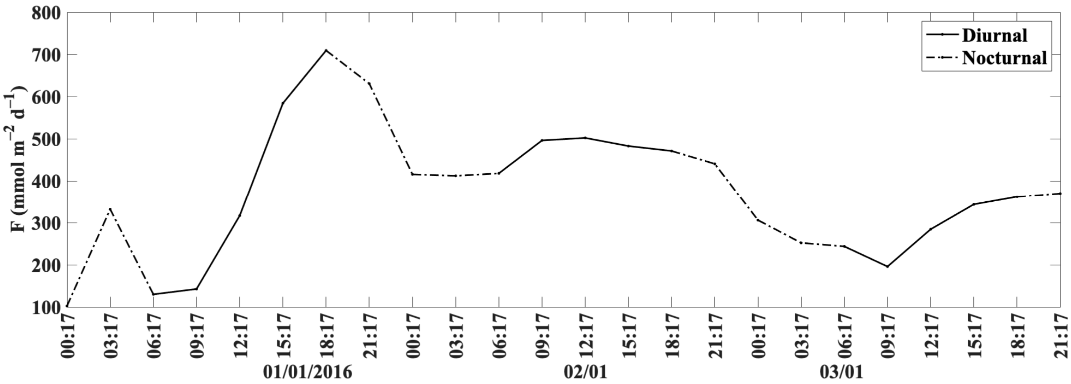

Figure 4. Sea–air CO_2 flux at station Kodiak (152°W, 57°N) from 1–3 January 2016. Diurnal hours are 06:00, 09:00, 12:00, and 15:00, and nocturnal hours are 18:00, 21:00, 00:00, and 03:00.

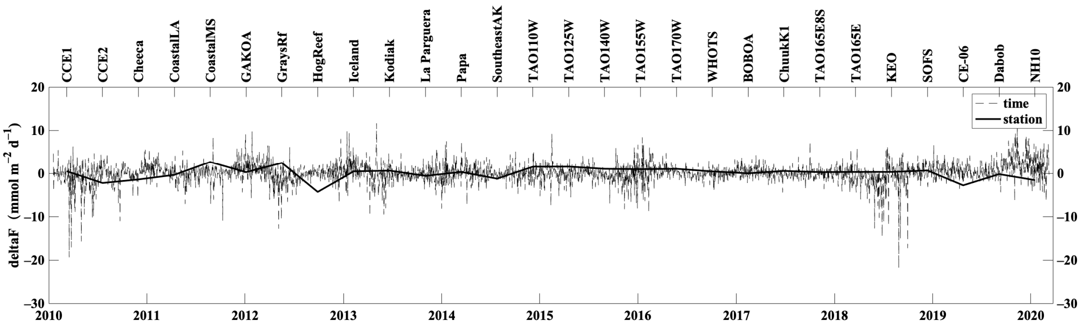

Figure 5. Average difference in the CO_2 flux calculated with and without the nocturnal effect at global buoy stations, with *deltaF* = $F_{real} - F_{day}$, the upper abscissa as the names of the global stations, and the lower abscissa as time. – shows the value corresponding to the time of the horizontal coordinate; — shows the value corresponding to the station of the horizontal coordinate.

3.2. Control Experiment on the Daily CO_2 Flux

To understand the main factors controlling the difference between CO_2 fluxes calculated using diurnal data and those calculated using diurnal–nocturnal data, a single-factor control experiment was conducted using buoy data from 2010 to 2020.

In the control experiment, the diurnal *SST*, *SSS*, wind speed, $pCO_{2\mathrm{w}}$, and $pCO_{2\mathrm{a}}$ data were used to calculate the daily CO_2 flux, thus obtaining F_{SST}, F_{SSS}, $F_{k_{660}}$, $F_{pCO_{2w}}$, and $F_{pCO_{2a}}$, respectively, where k_{660} is the gas transfer velocity k calculated using Sc of seawater at 20 °C (Sc = 660) and wind speed data. In each single-factor control experiment, the diurnal–nocturnal data were used to calculate the daily CO_2 flux, but the selected influencing factor was excluded from the calculation. The results of the control experiment are shown in Figure 6. The maximum $F_{pCO_{2w}} - F_{real}$ value from 2010 to 2020 was 1.21 mmol m^{-2} d^{-1}. The $F_{k_{660}} - F_{real}$ value, which indicated the influence of the daily variation in the second power of the wind speed on the calculation of the CO_2 flux, was also large, with a mean value of 0.312 mmol m^{-2} d^{-1}. Using only the diurnal data of $pCO_{2\mathrm{a}}$ to calculate the daily CO_2 flux also caused a considerable error of 0.157 mmol m^{-2} d^{-1}. The daily variation in *SSS* strongly affected the daily variation in L; however, this had little effect on the daily variation in the CO_2 flux. The influence of *SST* on L and Sc did not have a significant effect on the daily variation in the CO_2 flux (Figure 6). However, *SST* strongly influenced the daily variation in $pCO_{2\mathrm{w}}$, and in turn $pCO_{2\mathrm{w}}$ strongly influenced the daily variation in the CO_2 flux; therefore, *SST* significantly affected the diurnal variation in the CO_2 flux.

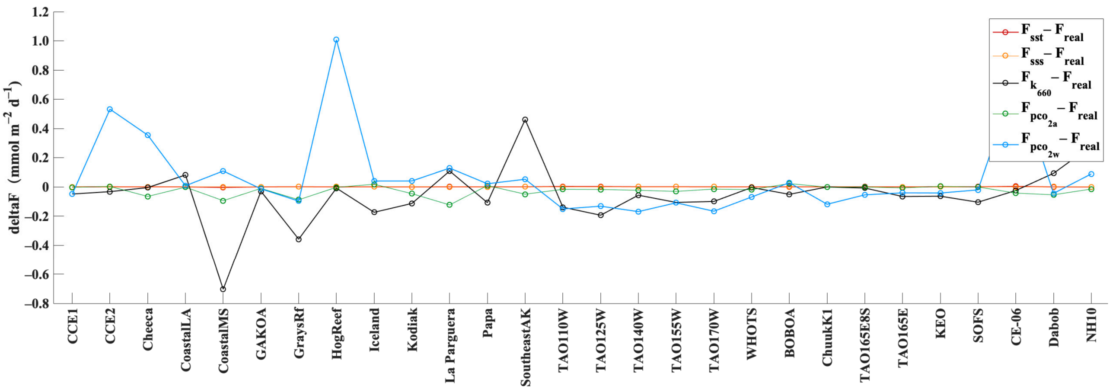

Figure 6. Effects of single factors on the calculated CO_2 flux at global stations from 2010 to 2020. The vertical coordinate is the difference between Freal and the CO_2 flux calculated after controlling for a single influencing factor.

As shown in Figure 6, there were clear differences between the $F_{pCO_{2w}}$ and F_{real} values at stations CCE2 (121°W, 34°N), Cheeca (80°W, 25°N), HogReef (64°W, 32°N), and CE-06 (125°W, 43°N). These stations were selected to consider the influence of each single factor on the calculation of the daily CO_2 flux over time. As shown in Figure 7, data from HogReef station covered the period from August 2016 to July 2018. The maximum and minimum $F_{pCO_{2w}} - F_{real}$ values were 21.77 mmol m^{-2} d^{-1} and 1.66×10^{-2} mmol m^{-2} d^{-1}, respectively. The daily CO_2 flux that was calculated using the diurnal pCO_{2w} data only corresponded to an overall decrease (increase) in the CO_2 sink (source) of the ocean; thus, the correction of pCO_{2w} resulted in a larger oceanic CO_2 sink and smaller oceanic CO_2 source values. The $F_{k_{660}} - F_{real}$ value exhibited an obvious seasonal variation, being smaller during October–November and May–July, with a minimum value of -7.75×10^{-4} mmol m^{-2} d^{-1}. Relatively large CO_2 fluxes were observed from December to April and from August to September, with a maximum of −26.71 mmol m^{-2} d^{-1}. Only diurnal wind data were used to calculate the daily CO_2 flux, which corresponded to increases in the CO_2 source and sink of the ocean. The sink value increased more than the source value.

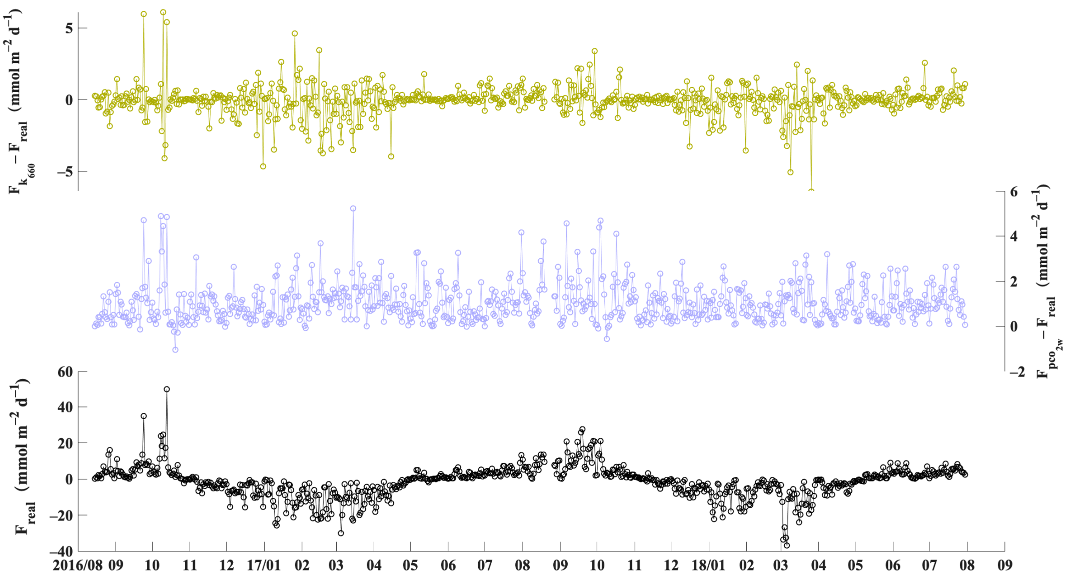

Figure 7. Differences in experimental CO_2 fluxes ($F_{k_{660}} - F_{\text{real}}$ and $F_{pCO_{2w}} - F_{\text{real}}$) and F_{real} at HogReef station from August 2016 to July 2018.

There were also significant differences between the $F_{k_{660}}$ and F_{real} values at stations CoastalMS (88°W, 30°N), GraysRf (81°W, 31°N), SoutheastAK (134°W, 56°N), and NH10 (124°W, 44°N). The results of the control experiment at SoutheastAK, where the difference between $F_{k_{660}}$ and F_{real} was large and the time series had the longest continuity, revealed that the influence of each factor on the error in the daily CO_2 flux calculation exhibited obvious seasonal differences. The $F_{k_{660}} - F_{real}$ values were lower from September to October and in March, with a minimum of -1.90×10^{-3} mmol m^{-2} d^{-1}, whereas higher values were observed from April to August and from November to February, with a maximum of 97.70 mmol m^{-2} d^{-1}. Although the CO_2 flux calculated using the diurnal data of each influencing factor was either larger or smaller than the daily CO_2 flux, with an obvious seasonal variation, this difference was not observable at all stations. When the diurnal data of each influencing factor were used to calculate the CO_2 flux, the calculated daily CO_2 flux from June to September increased at some stations, whereas it decreased at other stations. This was also the case from October to December and from January to May.

The daily variation in pCO_{2w} had a considerable influence on the daily variation in the CO_2 flux, and the SST value strongly influenced the daily variation in the CO_2 flux by affecting pCO_{2w} (when SSS was not considered). Although the daily variation in the wind speed also had a significant effect on the daily variation in the CO_2 flux, wind speed was not considered when establishing the nocturnal effect relationship because 24 h wind data were generally available. Therefore, it is recommended to use diurnal–nocturnal wind data to calculate the daily mean wind speed, and not to use the daytime wind data instead.

3.3. Nocturnal Effect Relationship

To eliminate the error caused by using diurnal data instead of diurnal–nocturnal data to calculate the CO_2 flux, we studied the relationship between diurnal and nocturnal CO_2 fluxes. The relationship between diurnal and nocturnal pCO_{2w} values is termed the nocturnal effect of pCO_{2w}, and the relationship between diurnal and nocturnal SST value is termed the nocturnal effect of SST. The nocturnal effects of pCO_{2w} and SST are collectively termed the nocturnal effect of the CO_2 flux. Diurnal and nocturnal CO_2 fluxes were calculated using diurnal and nocturnal data from various stations worldwide. The correlation coefficients between the calculated diurnal and nocturnal CO_2 fluxes were determined using a 99.9% significance test. As shown in Figure 8, the diurnal and nocturnal CO_2 fluxes were significantly correlated, with a correlation coefficient of 0.998 at station TAO155W (155°W, 0°N) in the Pacific Ocean. The weakest correlation (0.953) was observed at station NH10 (124°W, 44°N) in the Pacific Ocean. No obvious regional characteristics were observed between the location of stations in the global ocean (Figure 8) and the correlation coefficients between their diurnal–nocturnal mean CO_2 fluxes. Moreover, the correlation coefficients differed between proximate stations.

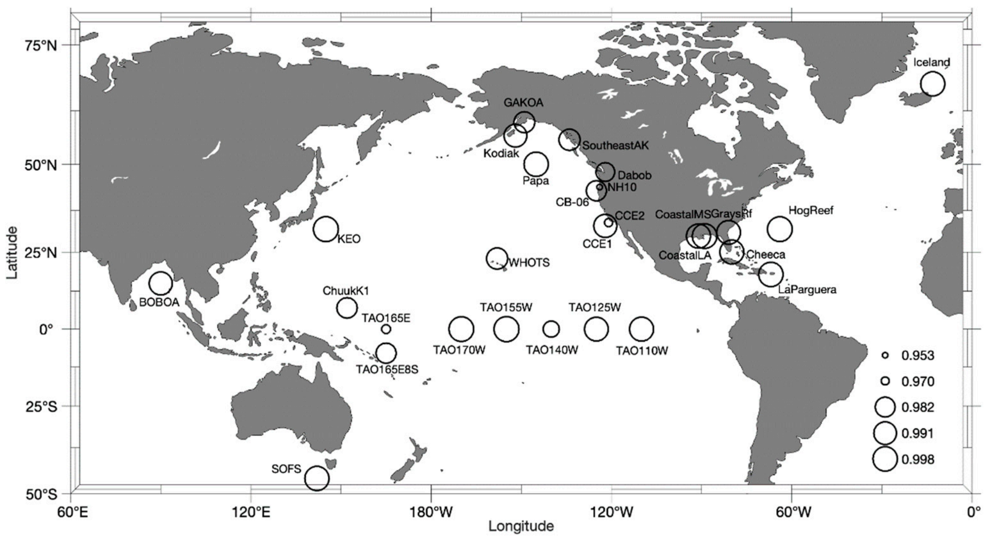

Figure 8. Spatial distribution of correlation coefficients between calculated diurnal and nocturnal CO_2 fluxes.

- Nocturnal effect of the pCO_2 of seawater

The nocturnal effect on the pCO_{2w} value was obtained from the fitting results in Figure 9a:

$$pCO_{2wn} = Y_1 \times pCO_{2wd} + Y_2 \tag{5}$$

where pCO_{2wn} is the nocturnal pCO_2 of seawater (μatm), pCO_{2wd} is the diurnal pCO_2 of seawater (μatm), Y_1 = 0.9898, and Y_2 = 3.0999.

- Nocturnal effect of SST

The nocturnal effect on the SST value was obtained from the fitting results in Figure 9b:

$$SST_n = Z_1 \times SST_d + Z_2 \tag{6}$$

where SST_n is the nocturnal SST (°C), SST_d is the diurnal SST (°C), Z_1 = 1.0012, and Z_2 = 0.0753.

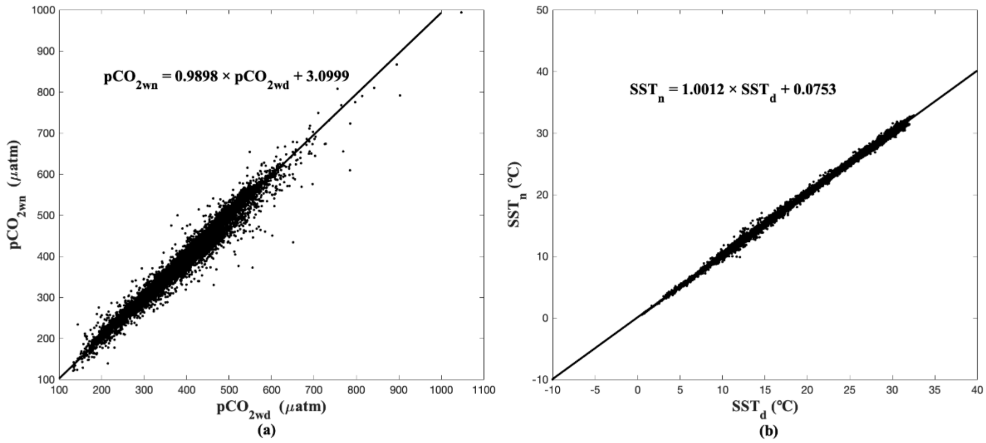

Figure 9. Fitting results of (**a**) nocturnal pCO_{2w} (pCO_{2wn}) and diurnal pCO_{2w} (pCO_{2wd}), and (**b**) nocturnal SST (SST_n) and diurnal SST (SST_d), whereby fitting results of using 75% of the data from 2010 to 2020.

- Daily variation in *Chl-a*

The *Chl-a* data from the Kiyomoto Yoko experiment (2003) are scarce and have little temporal continuity, and we chose the data with the longest temporal continuity to plot Figure 10. As no diurnal–nocturnal rule in *Chl-a* was observed (Figure 10), the nocturnal effect of *Chl-a* was not considered in this study. The *Chl-a* data is limited, so the conclusions may not be representative, and more *Chl-a* diurnal-nocturnal data is needed to support this conclusion. We couldn't obtain the nocturnal effect formula of *Chl-a* similar to SST (Equation (6)). So, we directly considered the nocturnal effects of pCO_{2w}. There were two obvious changes in the curve, which probably related to the change in the sampling station during the *Chl-a* experiment.

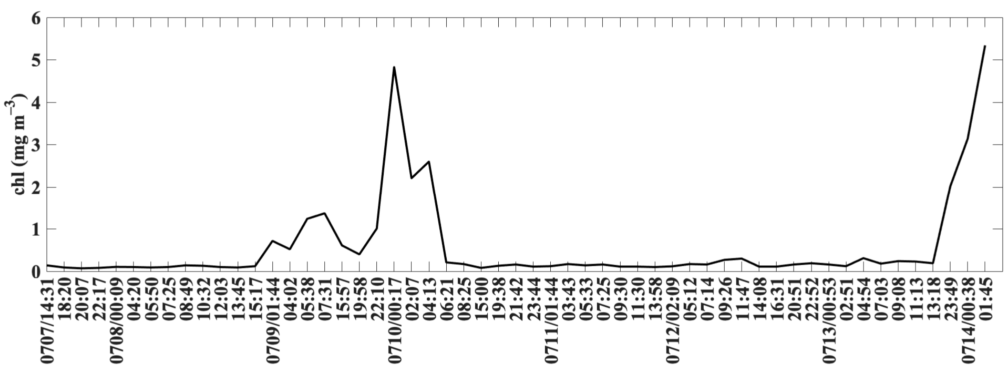

Figure 10. *Chl-a* data from the Kiyomoto_Yoko experiment (7–14 July 2003).

3.4. Comparison of Calculated and Real Daily CO_2 Fluxes

Equation (5) and pCO_{2wd} were used to calculate pCO_{2wn}, and the diurnal–nocturnal data of SSS, wind speed, pCO_{2a}, and SST_d were used to calculate the diurnal–nocturnal CO_2 flux (F_{comp}). In addition, Equation (6) and SST_d were used to calculate SST_n, and the diurnal–nocturnal data of SSS, wind speed, pCO_{2a}, and pCO_{2wd} were used to calculate the diurnal–nocturnal CO_2 flux (F_{comt}). By using Equations (5) and (6), SST_n and pCO_{2wn} were calculated based on SST_d and pCO_{2wd}, respectively, and the daily CO_2 flux was calculated by combining the diurnal–nocturnal data of SSS, wind speed, and pCO_{2a} (F_{com}). The F_{com}, F_{comp}, and F_{comt} values were compared with the F_{real} data using the root-mean-square error ($RMSE$):

$$RMSE = \sqrt{\frac{\sum_{i=1}^{n}[comF - F_{real}]^2}{n}} \tag{7}$$

where $comF$ is F_{comt}, F_{comp}, or F_{com}; F_{real} is the real daily CO_2 flux; and n is the number of data observations.

The results are shown in Figure 11, where F_{comp} is overlapped by F_{com} because the difference between F_{comp} and F_{com} was very small. The $RMSE$ values between F_{real} and F_{comt}, F_{comp}, F_{com}, and F_{day} were 12.58 mmol m^{-2} d^{-1}, 11.94 mmol m^{-2} d^{-1}, 11.93 mmol m^{-2} d^{-1}, and 46.32 mmol m^{-2} d^{-1}, respectively. Thus, compared with F_{day}, the values of F_{comt}, F_{comp}, and F_{com} were more accurate and closer to F_{real}. The similar $RMSE$ of F_{comt}, F_{comp}, and F_{com} indicate that there was a coincidence between the nocturnal effects of pCO_{2w} and SST. As SST is the most important influencing factor of pCO_{2w}, it is an important parameter for establishing the algorithm of pCO_{2w}.

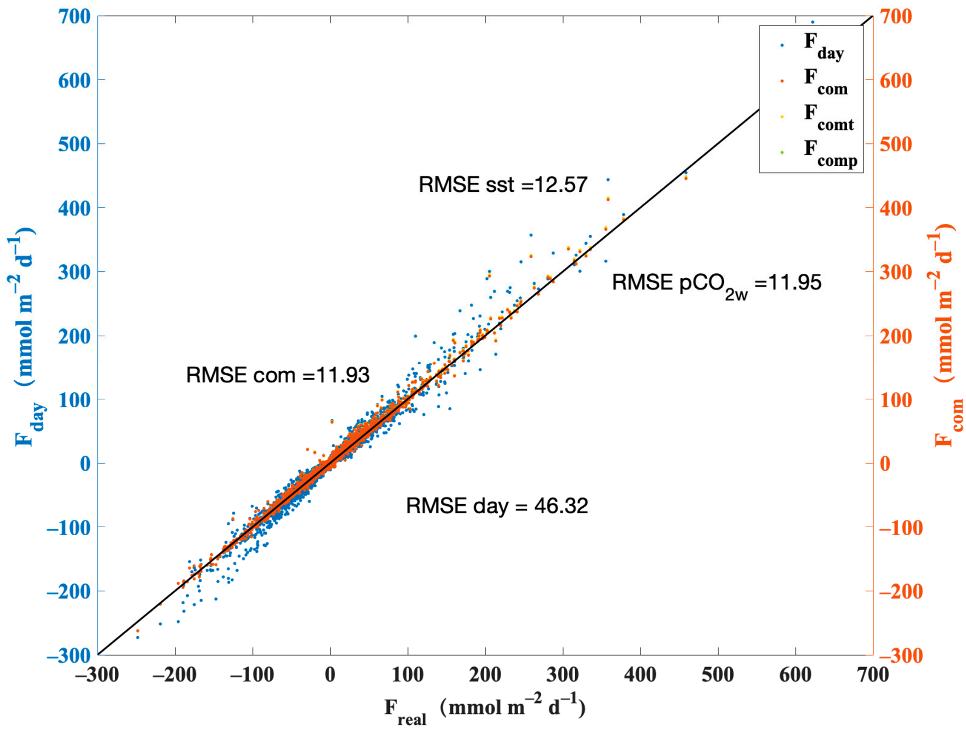

Figure 11. Results of using 25% of the data from 2010 to 2020 verify the calculated nocturnal effect.

3.5. Estimated Global CO_2 Flux

3.5.1. pCO_2 Remote Sensing Inversion Algorithm

As the remote sensing data of the SST and Chl-a parameters that correspond to the algorithm are solely diurnal, pCO_{2wd} and SST_d were used to develop a global pCO_{2w} algorithm as follows:

$$pCO_{2wd} = W_1 \times SST_d + W_2 \times ln(Chl{-}a) + W_3 \tag{8}$$

where SST_d is the absolute daily SST (°C) and *Chl-a* is the *Chl-a* concentration (mg m^{-3}) at the sea surface.

According to the fitting results in Figure 12a, W_1 = 3.40 in the $pCO_{2\mathrm{wd}}$ calculation model. The influence of SST on $pCO_{2\mathrm{wd}}$ was removed to obtain n$pCO_{2\mathrm{wd}}$. According to the fitting results in Figure 12b, W_2 = −4.44 and W_3 = 325.11 in the $pCO_{2\mathrm{wd}}$ calculation model.

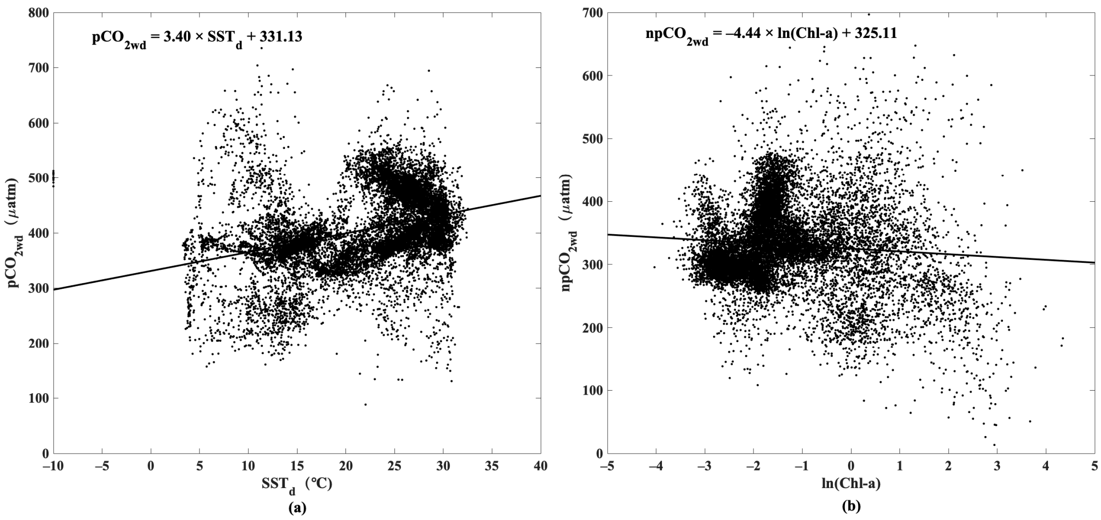

Figure 12. Fitting results of the global algorithm (2010–2020) between (**a**) $pCO_{2\mathrm{wd}}$ and SST_d, and (**b**) $pCO_{2\mathrm{wd}}$ with the temperature effect removed (n$pCO_{2\mathrm{wd}}$) and *Chl-a*.

Using all the buoy data, a $pCO_{2\mathrm{wd}}$ calculation model was established. The correlation coefficient between $pCO_{2\mathrm{wd}}$ and SST_d was 0.327 and passed the 99.9% significance test. The correlation coefficient between n$pCO_{2\mathrm{wd}}$ and *Chl-a* was 0.238 and also passed the 99.9% significance test. As the fitting effect was poor, the Pacific Ocean, Atlantic Ocean, and Indian Ocean sub-regions were selected to establish the calculation model.

According to the results in Figure 13, W_1 = 3.67, W_2 = 8.58, and W_3 = 346.94 in the $pCO_{2\mathrm{wd}}$ model of the Pacific Ocean sub-region. The correlation coefficient between $pCO_{2\mathrm{wd}}$ and SST_d was 0.369, while that between n$pCO_{2\mathrm{wd}}$ and *Chl-a* was −0.143. Both passed the 99.9% significance test. For the $pCO_{2\mathrm{wd}}$ model of the Atlantic Ocean sub-region, W_1 = 6.28, W_2 = −11.48, and W_3 = 231.98. The correlation coefficient between $pCO_{2\mathrm{wd}}$ and SST_d was 0.413, whereas that between n$pCO_{2\mathrm{wd}}$ and *Chl-a* was −0.392. Both passed the 99.9% significance test. For the $pCO_{2\mathrm{wd}}$ model of the Indian Ocean sub-region, W_1 = 12.96, W_2 = 0, and W_3 = 12.54. The correlation coefficient between $pCO_{2\mathrm{wd}}$ and SST_d was 0.826 and passed the 99.9% significant test; however, $pCO_{2\mathrm{wd}}$ was not correlated with *Chl-a*. Although the $pCO_{2\mathrm{wd}}$ model performed well for the Indian Ocean sub-region, the Pacific and Atlantic Ocean sub-regions had the strongest influence on the global $pCO_{2\mathrm{wd}}$ model.

3.5.2. Estimation of the CO_2 Flux Using the Nocturnal Effect

Remote sensing data of SST_d and *Chl-a* were used to calculate the $pCO_{2\mathrm{wd}}$($com\_pCO_{2\mathrm{wd}}$) for the $pCO_{2\mathrm{wd}}$ sub-region calculation model. In addition, $com\_pCO_{2\mathrm{wd}}$ was combined with the remote sensing data of SST_d and the diurnal data of SSS, $pCO_{2\mathrm{a}}$ and wind speed data were used to calculate the diurnal CO_2 flux (day_F_{com}). The corresponding ($com\_pCO_{2\mathrm{wn}}$) was calculated using Equation (5) and $com\_pCO_{2\mathrm{wd}}$, whereas the corresponding SST_n was calculated using Equation (6) and SST_d. Combining $com\_pCO_{2\mathrm{wd}}$, $com\_pCO_{2\mathrm{wn}}$, SST_d, and SST_n with the diurnal–nocturnal data of SSS, $pCO_{2\mathrm{a}}$, and wind speed, the CO_2 flux considering the nocturnal effect and $pCO_{2\mathrm{wd}}$ calculation model (cor_F_{com}) was calculated. The distribution of $cor\_F_{com} - day\_F_{com}$ is shown in Figure 14. The cor_F_{com} value was smaller than the day_F_{com} value at low latitudes, whereas it was greater at high latitudes. The $cor\_F_{com} - day\_F_{com}$ value also varied considerably with latitude, being smaller and greater at low and high latitudes, respectively.

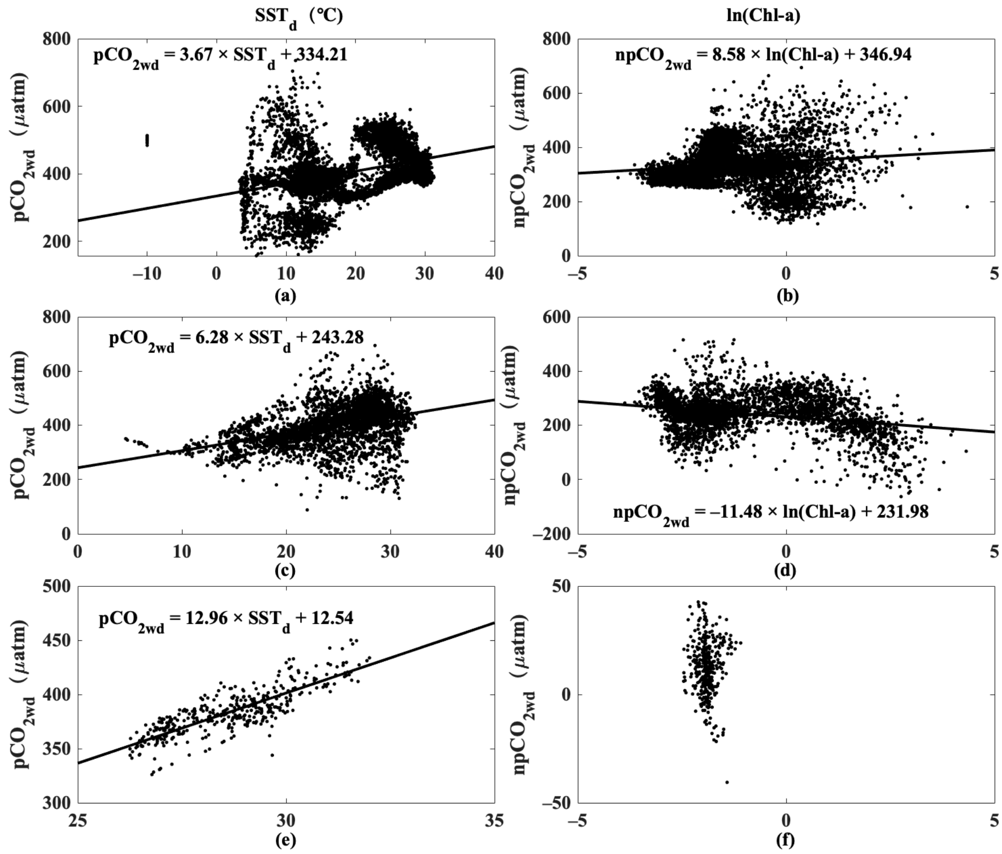

Figure 13. Regional algorithm for 2010–2020, showing the fitting results between $pCO_{2\text{wd}}$ and SST_d in the (**a**) Pacific, (**c**) Atlantic, and (**e**) Indian Ocean sub-regions; and between n$pCO_{2\text{wd}}$ and *Chl-a* in the (**b**) Pacific, (**d**) Atlantic, and (**f**) Indian Ocean sub-regions.

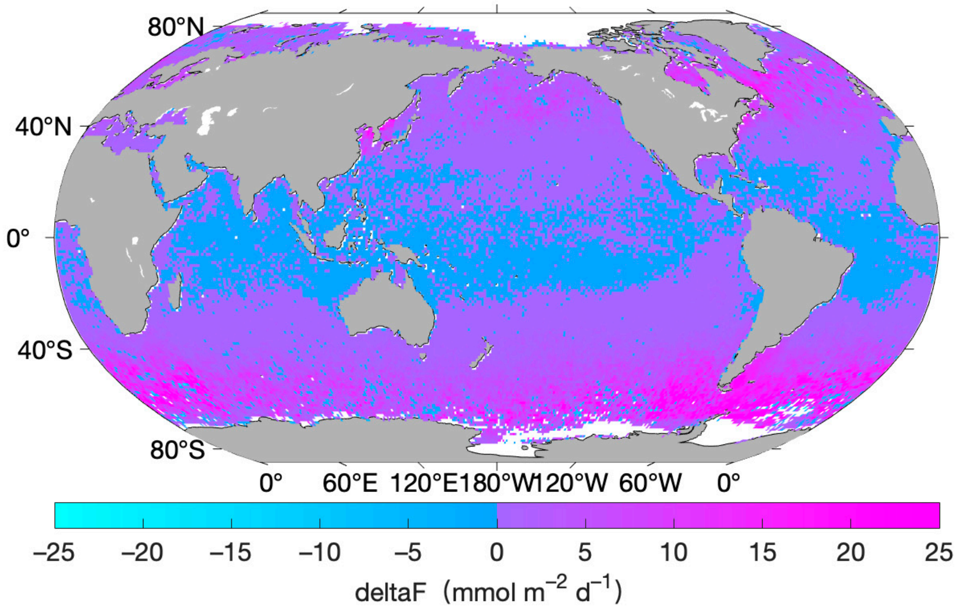

Figure 14. Global distribution of $cor\_F_{com} - day\_F_{com}$ (*deltaF*) from September 2020 to August 2021 (the flux calculation lacked data from 30 May to 20 June 2021 and from 22 to 27 June 2021).

As shown in Figure 14, the source and sink areas of CO_2 in the ocean were at low and high latitudes, respectively. The mean daily, monthly, and annual global CO_2 fluxes were -4.80×10^{-3} mmol m^{-2} d^{-1}, -23.36 mmol m^{-2} month^{-1}, and -6.86 mol m^{-2} y^{-1}, respectively, indicating that the global ocean acted as an overall sink of atmospheric CO_2 from September 2020 to August 2021.

As shown in Figures 14 and 15, compared with the use of *day_F*$_{com}$, the use of *cor_F*$_{com}$ decreased the source and sink amounts of oceanic CO_2. Specifically, compared with *day_F*$_{com}$, the global *cor_F*$_{com}$ value increased by 0.18 mmol m^{-2} d^{-1}, thereby *day_F*$_{com}$ overestimating the oceanic CO_2 sink by 10.21%. The mean monthly increase was 2.50 mmol m^{-2} month^{-1}, thus *day_F*$_{com}$ overestimating the mean oceanic CO_2 sink by 10.68%. The mean annual increase was 0.75 mol m^{-2} y^{-1}, thereby *day_F*$_{com}$ overestimating the mean oceanic CO_2 sink by 10.89%.

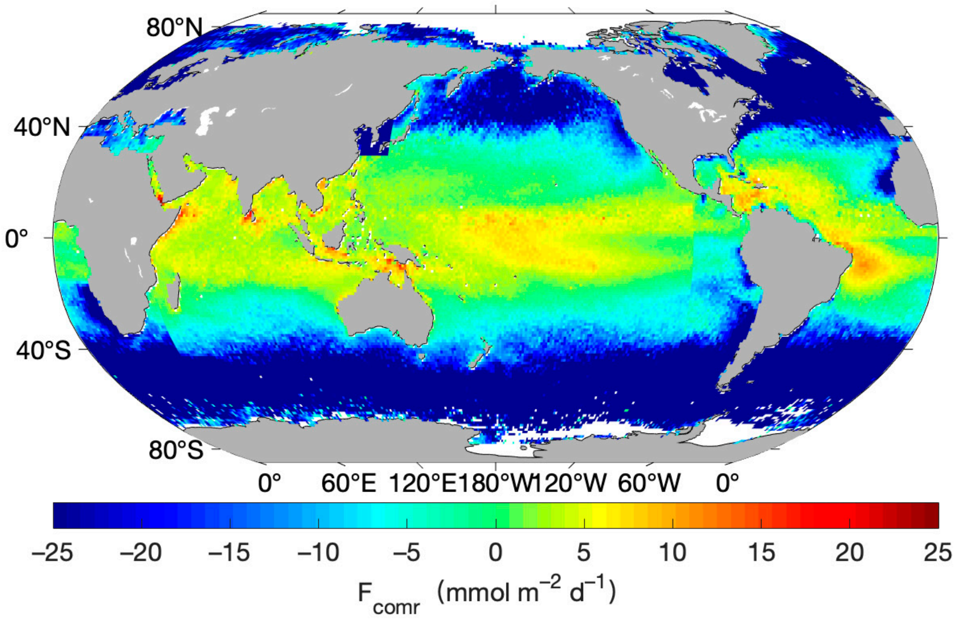

Figure 15. Distribution of CO_2 sources and sinks in the global ocean from September 2020 to August 2021.

For the convenience of understanding, we drew the flow diagram of the nocturnal effect establishment–checking–application, which is shown in Figure 16. There are many variable symbols in this paper, so we describe each of these in the accompanying Table A1.

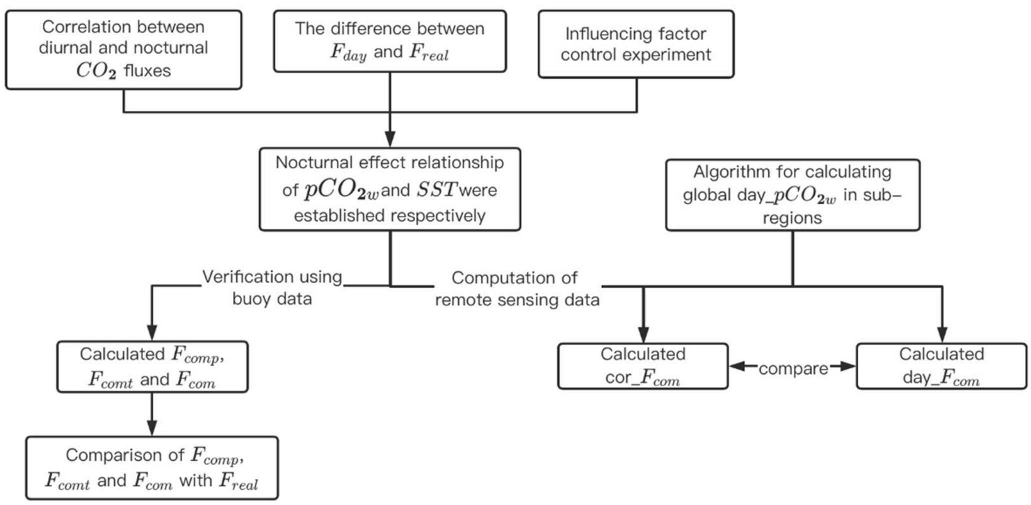

Figure 16. Research flow chart.

4. Conclusions

Calculating the daily CO_2 flux based on solely diurnal data of *SST*, *SSS*, wind speed, pCO_{2w}, and pCO_{2a} instead of the corresponding diurnal–nocturnal data can lead to significant errors. In this study, the mean $F_{day} - F_{real}$ value calculated based on buoy data from 2010 to 2020 was 0.0751 mmol m^{-2} d^{-1}. The corresponding CO_2 flux calculated using solely the diurnal data of *SST*, *SSS*, wind speed, pCO_{2w}, and pCO_{2a} increased or decreased the F_{real} value and exhibited obvious seasonal variations. The results of a control experiment showed that the daily variation in pCO_{2w} had the greatest influence on the daily variation in the CO_2 flux; therefore, the *SST* value, which influences the daily variation in pCO_{2w}, also significantly affected the daily variation in the CO_2 flux.

We found that the diurnal and nocturnal CO_2 fluxes were significantly correlated, with correlation coefficients of >0.950 based on a 99.9% significance test. In addition, the strength of the correlation was independent of the station location. To eliminate errors associated with using diurnal data instead of diurnal–nocturnal data to calculate the CO_2 flux, 75% of the randomly selected buoy data from 2010 to 2020 were used and the relationship between the nocturnal effects of *SST* and pCO_{2w} was established (Equations (5) and (6)). The nocturnal effect of the CO_2 flux was verified based on the remaining buoy data (i.e., 25%), and the *RMSE* values between F_{real} and F_{comt}, F_{comp}, F_{com}, and F_{day} were 12.58 mmol m^{-2} d^{-1}, 11.94 mmol m^{-2} d^{-1}, 11.93 mmol m^{-2} d^{-1}, and 46.32 mmol m^{-2} d^{-1}, respectively. Thus, F_{com} provided a more accurate estimation of F_{real} than did F_{day}. The results indicate that the error associated with using diurnal data instead of diurnal–nocturnal data to calculate the CO_2 flux can be reduced by accounting for the nocturnal effect.

As the *SST* value was the most important factor influencing pCO_{2w}, the nocturnal effects of these parameters partially coincided. In contrast, no obvious diurnal–nocturnal relationship was observed for *Chl-a*; thus, the nocturnal effect of *Chl-a* was not considered in this study. Although the daily variation in the wind speed significantly affected the daily variation in the CO_2 flux, this parameter was not considered when we established the relationship of the nocturnal effect because 24 h wind data can usually be obtained.

The fitting effect of using the complete set of buoy data to build the pCO_{2wd} model was poor; therefore, we chose to build the pCO_{2wd} models based on data for the Pacific Ocean, Atlantic Ocean, and Indian Ocean, respectively. The Pacific and Atlantic Ocean sub-regions played major roles in the regional algorithmic model. The pCO_{2wd} of the Indian Ocean was only related to SST_d, and the fitting results between pCO_{2wd} and SST_d were good. However, the algorithm for the Indian Ocean was only based on one station (BOBOA) from 2013 to 2017 because there was insufficient data for stations in the Indian Ocean. In the future, we hope to obtain more relevant data for the Indian Ocean to further improve the algorithmic modelling of this region.

The global CO_2 flux was calculated using the pCO_{2wd} model and the established nocturnal effect. The source and sink areas of CO_2 in the global ocean were at low and high latitudes, respectively. The mean daily, monthly, and annual global CO_2 fluxes were -4.80×10^{-3} mmol m^{-2} d^{-1}, -23.36 mmol m^{-2} $month^{-1}$, and -6.86 mol m^{-2} y^{-1}, respectively, indicating that the global ocean was an overall sink for atmospheric CO_2 from September 2020 to August 2021. During this period, the oceanic sources and sinks of CO_2 determined based on cor_F_{com} were smaller than those based on day_F_{com}. Compared with day_F_{com}, the global cor_F_{com} value was greater by 0.18 mmol m^{-2} d^{-1}, thereby day_F_{com} overestimating the oceanic CO_2 sink by 10.21%. The mean monthly increase of cor_F_{com} was 2.50 mmol m^{-2} $month^{-1}$, thus day_F_{com} overestimating the mean oceanic CO_2 sink by 10.68%. The mean annual increase of cor_F_{com} was 0.75 mol m^{-2} y^{-1}, thus day_F_{com} overestimating the mean oceanic CO_2 sink by 10.89%.

In the current studies, the pCO_{2W} algorithms were frequently built using data from small regions, and few algorithms were built from large areas. However, in order to estimate the global CO_2 flux using satellite data, a large-scale algorithm was used, which was not so accurate as the small-scale regional algorithms. We will improve the accuracy of the global-scale pCO_{2W} algorithm to further refine the process of estimating global daily CO_2 fluxes in future studies. The equation for calculating the k used to determine the CO_2 flux is one of the many parameterised formulas that have been developed for establishing the relationship between the k of CO_2 and wind speed. Different k equations will yield different CO_2 fluxes. Although such differences were not considered in this study, we hope to address them in future studies.

Author Contributions: Conceptualization, T.Y. and R.J.; Methodology, T.Y. and R.J.; Software, R.J.; Validation, B.T., W.S. and S.H.; Formal Analysis, W.S.; Investigation, R.J.; Resources, T.Y.; Data Curation, R.J. and T.Y.; Writing—Original Draft Preparation, R.J. and T.Y.; Writing—Review & Editing, T.Y.; Visualization, R.J.; Supervision, B.T., W.S., S.H. and Y.W.; Project Administration, T.Y.; Funding Acquisition, T.Y. All authors have read and agreed to the published version of the manuscript.

Funding: This work was supported by National Natural Science Foundation of China (Grant No. 41906152, No. 42176012, No. 42130402), the Key Special Project for Introduced Talents Team of Southern Marine Science and Engineering Guangdong Laboratory (Guangzhou) (Grant No. GML2019ZD0602), the Global Change and Air-Sea Interaction II Program (Grant No. GASI-01-DLYG-WIND02 and No. GASI-01-DLYG-EPAC0) and the National Key Research and Development Program of China (2021YFC3101702).

Data Availability Statement: Publicly available datasets were analyzed in this study. These data can be found here: [https://www.ncei.noaa.gov/, accessed on 8 May 2022; https://cds.climate.copernicus.eu/, accessed on 8 May 2022; https://oceandata.sci.gsfc.nasa.gov/, accessed on 8 May 2022; https://disc.gsfc.nasa.gov/, accessed on 8 May 2022; https://resources.marine.copernicus.eu/, accessed on 8 May 2022].

Acknowledgments: We thank the Ocean Carbon Data System (OCADS) for providing the pCO_2, *SST*, and *SSS* data (https://www.ncei.noaa.gov/access/ocean-carbon-data-system/oceans/time_series_moorings.html), NASA for providing the *SST* and chlorophyll data and for making the data available systematically (https://oceandata.sci.gsfc.nasa.gov/directaccess/MODIS-Aqua/L3SMI/), the fifth-generation European Centre for Medium-Range Weather Forecasts (ECMWF) for providing the wind and atmospheric pressure data (https://cds.climate.copernicus.eu/cdsapp#!/dataset/reanalysis-era5-single-levels?tab=overview), Copernicus Marine Service for providing the *SSS* data (https://marine.copernicus.eu), and Earthdata for providing the atmospheric CO_2 and water vapour data (https://disc.gsfc.nasa.gov/datasets/SNDRAQIL3CDCCP_2/summary?keywords=CO2); accessed date: 8 May 2022.

Conflicts of Interest: The authors declare no conflict of interest.

Appendix A

Table A1. Variable symbols in this article defined in the corresponding table.

Quantity	Meaning
pCO_{2w}	Partial pressure of CO_2 in seawater
pCO_{2a}	Partial pressure of CO_2 in air
F_{day}	The CO_2 flux calculated using diurnal buoy data
F_{real}	The CO_2 flux calculated using diurnal–nocturnal buoy data
F_{SST}	The daily CO_2 flux calculated using diurnal *SST* buoy data only, and other parameters except *SST* were diurnal–nocturnal buoy data
F_{SSS}	The daily CO_2 flux calculated using diurnal *SSS* buoy data only, and other parameters except *SSS* were diurnal–nocturnal buoy data
$F_{k_{660}}$	The daily CO_2 flux calculated using diurnal wind speed buoy data only, and other parameters except wind speed were diurnal–nocturnal buoy data
$F_{pCO_{2w}}$	The daily CO_2 flux calculated using diurnal pCO_{2w} buoy data only, and other parameters except pCO_{2w} were diurnal–nocturnal buoy data
$F_{pCO_{2a}}$	The daily CO_2 flux calculated using diurnal pCO_{2a} buoy data only, and other parameters except pCO_{2a} were diurnal–nocturnal buoy data
pCO_{2wn}	The nocturnal pCO_{2w}. This variable was used to establish the nocturnal relationship using buoy data

Table A1. *Cont.*

Quantity	Meaning
$pCO_{2\mathrm{wd}}$	The diurnal $pCO_{2\mathrm{w}}$. This variable was used to establish the nocturnal relationship using buoy data
SST_n	The nocturnal *SST*. This variable was used to establish the nocturnal relationship using buoy data
SST_d	The diurnal *SST*. This variable was used to establish the nocturnal relationship using buoy data
F_{comp}	The CO_2 flux calculated using only the nocturnal effect for $pCO_{2\mathrm{w}}$ and satellite data for each parameter
F_{comt}	The CO_2 flux calculated using only the nocturnal effect for *SST* and satellite data for each parameter
F_{com}	The CO_2 flux calculated using only the nocturnal effect for $pCO_{2\mathrm{w}}$ and *SST* and satellite data for each parameter
$com\_pCO_{2\mathrm{wd}}$	$pCO_{2\mathrm{wd}}$ calculated using remote sensing data of SST_d and *Chl-a*
$com\_pCO_{2\mathrm{wn}}$	The $pCO_{2\mathrm{wn}}$ calculated using the nocturnal effect for $pCO_{2\mathrm{w}}$ and $com\_pCO_{2\mathrm{wd}}$
day_F_{com}	The diurnal CO_2 flux calculated using diurnal remote sensing data of *SSS*, $pCO_{2\mathrm{a}}$ and wind speed and remote sensing data of SST_d and $com\_pCO_{2\mathrm{wd}}$
cor_F_{com}	The diurnal–nocturnal CO_2 flux calculated combining $com\_pCO_{2\mathrm{wd}}$, $com\_pCO_{2\mathrm{wn}}$, SST_d, and SST_n with the diurnal–nocturnal remote sensing data of *SSS*, $pCO_{2\mathrm{a}}$, and wind speed, considering the nocturnal effect

References

1. Friedlingstein, P.; Allen, M.; Canadell, J.G.; Peters, G.P.; Seneviratne, S.I. Comment on "The global tree restoration potential". *Science* **2019**, *366*, eaay8060. [CrossRef] [PubMed]
2. Sarmiento, J.L.; Gloor, M.; Gruber, N.; Beaulieu, C.; Jacobson, A.R.; Mikaloff, F.; Pacala, S.; Rodgers, K. Trends and regional distributions of land and ocean carbon sinks. *Biogeosciences* **2010**, *7*, 2351–2367. [CrossRef]
3. Archer, D.; Kheshgi, H.; Maier-Reimer, E. Multiple timescales for neutralization of fossil fuel CO_2. *Geophys. Res. Lett.* **1997**, *24*, 405–408. [CrossRef]
4. Yu, T. *A Study on the Inversion Algorithms of Air-Sea CO_2 Transfer Velocity and Flux from Satellite Data*; University of Chinese Academy of Sciences: Beijing, China, 2013. (In Chinese)
5. Landschützer, P.; Laruelle, G.G.; Roobaert, A.; Regnier, P. A uniform pCO_2 climatology combining open and coastal oceans. *Earth Syst. Sci. Data* **2020**, *12*, 2537–2553. [CrossRef]
6. Bai, Y.; Cai, W.J.; He, X.; Zhai, W.; Pan, D.; Dai, M.; Yu, P. A mechanistic semi-analytical method for remotely sensing sea surface pCO_2 in river-dominated coastal oceans: A case study from the East China Sea. *J. Geophys. Res. Ocean.* **2015**, *120*, 2331–2349. [CrossRef]
7. Brisson, A.; Le Borgne, P.; Marsouin, A. Results of One Year of Preoperational Production of Sea Surface Temperatures from GOES-8. *J. Atmos. Ocean. Technol.* **2010**, *19*, 1638–1652. [CrossRef]
8. Kettle, H.; Merchant, C.; Jeffery, C.; Filipiak, M.; Gentemann, C. The impact of diurnal variability in sea surface temperature on the central Atlantic air-sea CO_2 flux. *Atmos. Chem. Phys.* **2009**, *9*, 529–541. [CrossRef]
9. Woolf, D. The response to phase-dependent wind stress and cloud fraction of the diurnal cycle of *SST* and air–sea CO_2 exchange. *Ocean. Model.* **2008**, *23*, 33–48.
10. Lu, Z. *Diurnal Variations of Sea Surface pCO_2 and the Controls in Coastal Seas*; Xiamen University: Xiamen, China, 2009. (In Chinese)
11. Jeffery, C.D.; Woolf, D.K.; Robinson, I.S.; Donlon, C.J. One-dimensional modelling of convective CO_2 exchange in the Tropical Atlantic. *Ocean. Model.* **2007**, *19*, 161–182. [CrossRef]
12. Hare, J.E.; Fairall, C.W.; McGillis, W.R.; Edson, J.B.; Ward, B.; Wanninkhof, R. Evaluation of the National Oceanic and Atmospheric Administration/Coupled-Ocean Atmospheric Response Experiment (NOAA/COARE) air-sea gas transfer parameterization using GasEx data. *J. Geophys. Res. Ocean.* **2004**, *109*, C08S11. [CrossRef]
13. Michel, S.; Hapron, B.C.; Tournadre, J.; Reul, N. Sea surface salinity variability from a simplified mixed layer model of the global ocean. *Ocean. Sci. Discuss.* **2007**, *4*, 41–106.
14. Marrec, P.; Cariou, T.; Latimier, M.; Macé, E.; Morin, P.; Vernet, M.; Bozec, Y. Spatio-temporal dynamics of biogeochemical processes and air-sea CO_2 fluxes in the Western English Channel based on two years of FerryBox deployment. *J. Mar. Syst.* **2014**, *140*, 26–38. [CrossRef]
15. Borges, A.V.; Frankignoulle, M. Daily and seasonal variations of the partial pressure of CO_2 in surface seawater along Belgian and southern Dutch coastal areas. *J. Mar. Syst.* **1999**, *19*, 251–266. [CrossRef]
16. Bates, N.R.; Samuels, L.; Merlivat, L. Biogeochemical and physical factors influencing seawater fCO_2 and air-sea CO_2 exchange on the Bermuda coral reef. *Limnol. Oceanogr.* **2001**, *46*, 833–846. [CrossRef]

17. Fransson, A.; Chierici, M.; Anderson, L.G. Diurnal variability in the oceanic carbon dioxide system and oxygen in the Southern Ocean surface water. *Deep. Sea Res. Part II Top. Stud. Oceanogr.* **2004**, *51*, 2827–2839. [CrossRef]
18. Kuss, J.; Roeder, W.; Wlost, K.P.; Degrandpre, M. Time-series of surface water CO_2 and oxygen measurements on a platform in the central Arkona Sea (Baltic Sea): Seasonality of uptake and release. *Mar. Chem.* **2006**, *101*, 220–232. [CrossRef]
19. Colas, F.; McWilliams, J.C.; Capet, X.; Kurian, J. Heat balance and eddies in the Peru-Chile current system. *Clim. Dyn.* **2011**, *39*, 509–529. [CrossRef]
20. Zhurbas, V.; And, J.L.; Vahtera, E. Modeling of the mesoscale structure of coupled upwelling/downwelling events and the related input of nutrients to the upper mixed layer in the Gulf of Finland, Baltic Sea. *J. Geophys. Res. Ocean.* **2008**, *113*, C05004. [CrossRef]
21. Piedracoba, S.; Nieto-Cid, M.; Teixeira, G.; Garrido, J.L.; Alvarez-Salgado, X.A.; Roson, G.; Castro, C.G.; Perez, F.F. Physical-biological coupling in the coastal upwelling system of the Ria de Vigo (NW Spain). II: In vitro approach. *Mar. Ecol. Prog. Ser.* **2008**, *353*, 41–53. [CrossRef]
22. Rutgersson, A.; Smedman, A. Enhanced air–sea CO_2 transfer due to water-side convection. *J. Mar. Syst.* **2010**, *80*, 125–134. [CrossRef]
23. Norman, M.; Rutgersson, A.; Sahlée, E. Impact of improved air–sea gas transfer velocity on fluxes and water chemistry in a Baltic Sea model. *J. Mar. Syst.* **2013**, *111–112*, 175–188. [CrossRef]
24. Wimart-Rousseau, C.; Lajaunie-Salla, K.; Marrec, P.; Wagener, T.; Raimbault, P.; Lagadec, V.; Lafont, M.; Garcia, N.; Diaz, F.; Pinazo, C. Temporal variability of the carbonate system and air-sea CO_2 exchanges in a Mediterranean human-impacted coastal site. *Estuar. Coast. Shelf Sci.* **2020**, *236*, 106641. [CrossRef]
25. Frankignoulle, M. Field measurements of air-sea CO_2 exchange1. *Limnol. Oceanogr.* **1988**, *33*, 313–322. [CrossRef]
26. Takahashi, T.; Sutherland, S.C.; Wanninkhof, R.; Sweeney, C.; Feely, R.A.; Chipman, D.W.; Hales, B.; Friederich, G.; Chavez, F.; Sabine, C.; et al. Climatological mean and decadal change in surface ocean pCO_2, and net sea-air CO_2 flux over the global oceans. *Deep. Sea Res. Part II Top. Stud. Oceanogr.* **2008**, *56*, 554–577. [CrossRef]
27. Wanninkhof, R. Relationship between wind speed and gas exchange over the ocean revisited. *Limnol. Oceanogr. Methods* **2014**, *12*, 351–362. [CrossRef]
28. Weiss, R.F. Carbon dioxide in water and seawater: The solubility of a non-ideal gas. *Mar. Chem.* **1974**, *2*, 203–215. [CrossRef]